Harmonic-potential traps for indirect excitons in coupled quantum wells

V. Negoita and D. W. Snoke*
Department of Physics and Astronomy, University of Pittsburgh, 3941 O'Hara Street, Pittsburgh, Pennsylvania 15260

K. Eberl
Max-Planck-Institut für Festkörperforschung, Heisenbergstrasse 1, 70506 Stuttgart, Germany
(Received 14 September 1998; revised manuscript received 18 March 1999)

We explain our method of creating an in-plane harmonic potential for indirect excitons in coupled quantum wells, which has been developed for experiments on Bose condensation of excitons in two dimensions, although this method may also be used for trapping a two-dimensional electron gas. The indirect excitons in our coupled quantum wells exhibit a Stark shift of over 60 meV and lifetime of approximately 100 ns when electric field is applied normal to the wells. The excitons also move in response to applied voltage as if they had charge, with an effective mobility of 800 cm^2/V s. We find that the effects of screening of the electric field at high carrier density are very important for understanding the behavior of the excitons.
[S0163-1829(99)00228-3]

I. INTRODUCTION

Over the past 15 years, several experiments have indicated evidence of Bose effects or Bose condensation of excitons in semiconductors.[1–13] One common element of all of these experiments has been that the exciton or biexciton gas is created by a laser in a particular spot, and then the gas freely expands out of this excitation region. This experimental geometry leads to a particular problem for studies of Bose condensation: exactly what is the ground state of the system into which the particles should condense? Presumably, a ''local'' ground state can be defined, similar to the way that superfluid helium can remain in a quasiequilibrium ground state even while it flows from one region of a vessel to another. One does not expect that the exciton gas must fill the entire crystal before it can condense. Nevertheless, the lack of a well-defined ground state forces all of these studies to deal with *hydrodynamics* of excitons, a topic still not well understood, in part because the excitons couple strongly to hot phonons.

By contrast, the recent experiments with alkali atoms in magneto-optical traps[14,15] have produced a dramatic telltale of Bose condensation, namely, a *spatial* condensation into a two-component distribution, with the condensate particles in a well-defined ground state, which is possible because the atoms lie trap with a nearly harmonic potential. It has long been known[16] that excitons in a harmonic potential will also show this behavior if they undergo Bose condensation; a method of creating a harmonic potential for excitons in bulk semiconductors is well established,[16] but so far, experimental attempts with bulk semiconductors have not succeeded in creating a density of excitons high enough for Bose condensation in this kind of trap.

Our goal has been to try to produce this kind of trap in a system of two-dimensional excitons, known as indirect, or ''dipole,'' excitons. This system is appealing because (1) the excitons can have long lifetimes due to the spatial separation of the electron and hole, (2) the interaction between the dipole-aligned excitons is strongly repulsive, so that a Fermi-liquid state is not expected at high density, and (3) the quality of semiconductor heterostructures has been steadily increasing, so that true two-dimensional physics can be studied. In a true two-dimensional system, Bose-Einstein condensation is not expected, but rather a Kosterlitz-Thouless transition to a superfluid state[17] (although Fernández-Rossier, Tejedor, and Merlin[18] have recently argued that the coupling of the excitons to the photon states will allow them to undergo Bose condensation in two dimensions.) When even a small confining potential is created in two dimensions, however, then Bose condensation in two dimensions is possible.[19] Zhu, Littlewood, and Rice[20] have recently examined a scenario like this, in which indirect excitons are confined to a trap.

Early experiments with this type of exciton[7] showed evidence for Bose effects, but later work[21] showed that localization due to random variations in the structures significantly complicated the analysis of the luminescence lineshape. More recent studies of similar structures[8,9] have shown quite promising results, including evidence for increased diffusion out of the excitation region at high density and low temperature. Other recent measurements of the diffusion of indirect excitons have also shown fast expansion at high densities.[22] Enhanced diffusion is expected for superfluid excitons,[23] but can also be attributed to other, classical effects which also occur at high density, such as phonon wind.[24] By contrast, if the excitons move *inward* toward the center of the excitation region due to a confining potential, no classical effect can reproduce this effect.

A well-defined confining potential is also important for tests of phase coherence of the exciton condensate. Recently, several authors[18,25,26] have proposed optical probes of the phase coherence of the exciton condensate. Underlying all these approaches is the fact that Bose condensation implies spontaneous phase coherence, and since excitons couple to photon states, this phase coherence should transfer to the photons, even in the absence of lasing. Confining the excitons to a trap is much more amenable to these kinds of tests than allowing free expansion of the exciton gas, since the

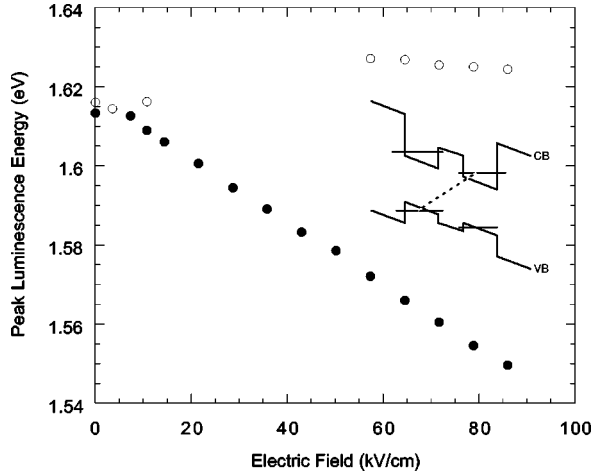

FIG. 1. Peak photon energy of the two luminescence lines from the structure, as a function of electric field relative to the flat-band field. Solid circles: indirect (interwell) excitons, open circles: direct (intrawell) excitons. Inset: Band structure of the coupled quantum well structures used in this experiment. Indirect excitons are formed from electrons in the lowest conduction subband and the highest valence subband.

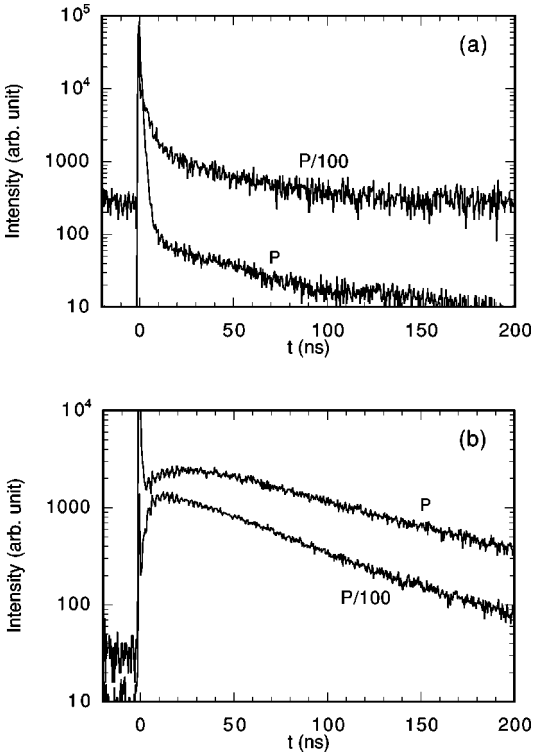

FIG. 2. (a) Total intensity of the direct exciton luminescence line, integrated spatially over the entire excitation area and integrated spectrally over the range $\lambda = 758$ to 768 nm, from a coupled quantum well sample with an electric field of 42 kV/cm with the sample immersed in superfluid helium at $T = 2$ K, as a function of time following a short (5 ps) laser pulse at 620 nm, for two laser excitation powers. Full power (P) corresponds to 3.0×10^3 W/cm^2. (b) Total intensity of the indirect exciton luminescence line under the same conditions and for the same two excitation intensities, integrated spatially over the excitation area and integrated spectrally over the range $\lambda = 779$ to 789 nm. The very short lifetime signal at early time is due to hot carrier luminescence from the substrate. The curves in both (a) and (b) at different powers have been shifted by an overall multiplicative factor to avoid overlap.

ground state in a harmonic potential is well defined.

As previously reported,[27] we have succeeded at creating a harmonic-potential minimum for indirect excitons in a two-dimensional plane. In this paper we discuss in detail the physical considerations which come in to these experiments.

II. CHARACTERISTICS OF INDIRECT EXCITONS IN COUPLED QUANTUM WELLS

The samples we used were GaAs/Al_xGa_{1-x}As coupled quantum well structures fabricated via molecular-beam epitaxy (MBE) at the Max-Planck-Institute in Stuttgart; the substrate is heavily *p*-doped and the capping layer is heavily n-doped in order to allow electric field perpendicular to plane of the quantum wells; the intrinsic field due to the doping is approximately 21 kV/cm. Five sets of coupled quantum wells are created which consist of two 60 Å undoped GaAs wells with a 42 Å $Al_{0.3}Ga_{0.7}As$ barrier between them, with 200 Å pure AlAs barriers in between the sets of coupled quantum wells to prevent any coupling between them. The inset of Fig. 1 illustrates the band structure when electric field is applied; ''indirect'' excitons are formed from electrons and holes in different quantum wells, while ''direct'' excitons are formed from electrons and holes in the same well. Figure 1 gives the energy of the luminescence lines as a function of the electric field. As the electric field is increased, the energy of the indirect excitons undergoes a strong Stark shift to lower energy, as also seen in previous studies (e.g., Refs. 28–30). The spatial separation of electron and hole into two separate planes also increases the lifetime of the excitons; in our samples we measure lifetimes of the indirect excitons of around 100 ns at high applied voltage, as seen at late times in Fig. 2.

The behavior of the luminescence at early times in Fig. 2 indicates that the analysis of the luminescence is more complicated than one might first expect. The direct exciton luminescence shows an initial fast decay, while the indirect exciton luminescence rises initially. One might interpret this behavior simply in terms of conversion from the upper, direct exciton species down into the lower, indirect exciton species, but the density dependence of the curves gives a more complicated picture. The initial decay time of the upper line is much *faster* at higher power, while the initial rise time of the lower line is *slower* at higher power. Looking at the luminescence spectra as a function of time helps us to understand this behavior. As seen in Fig. 3, the energy of the lower, indirect exciton line shifts strongly over time following the laser pulse. We interpret this shift as due to the effect of screening of the electric field at early times when the carrier density is high; both the excitons themselves as well as free carriers can contribute to screening out the applied field. This screening reduces the effective field felt by the excitons for up to 75 ns after the laser pulse; as seen in Fig. 3(b), the blueshift of the indirect exciton line relaxes back to the unscreened position with a time constant of about 25 ns.

One might posit that the blueshift is due to the mean-field renormalization of the exciton level due to the repulsive in-

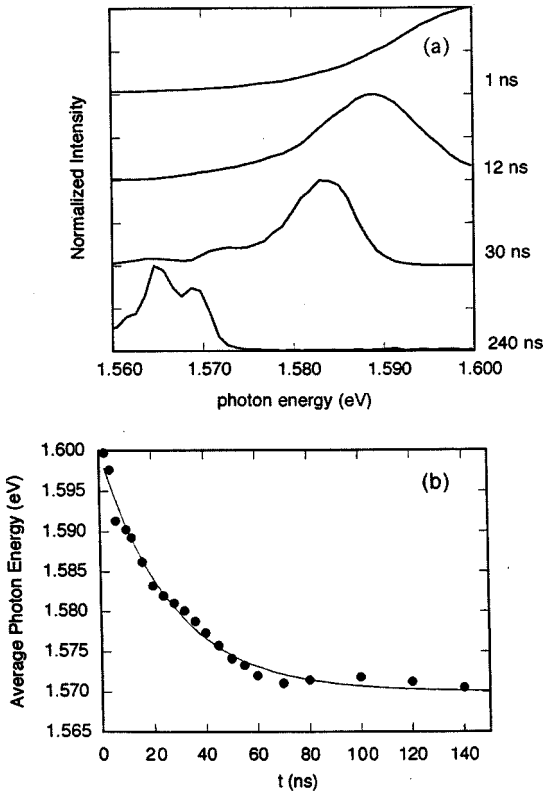

FIG. 3. (a) Indirect exciton luminescence spectrum at various times following an intense (25 nJ), short (5 ps) laser pulse at 660 nm, for 60 kV/cm applied field, with $T=6$ K. (b) Average photon energy of the data shown in (a) as a function of time. The solid line is a fit to a single exponential decay of the energy shift with $\tau = 26.5$ ns.

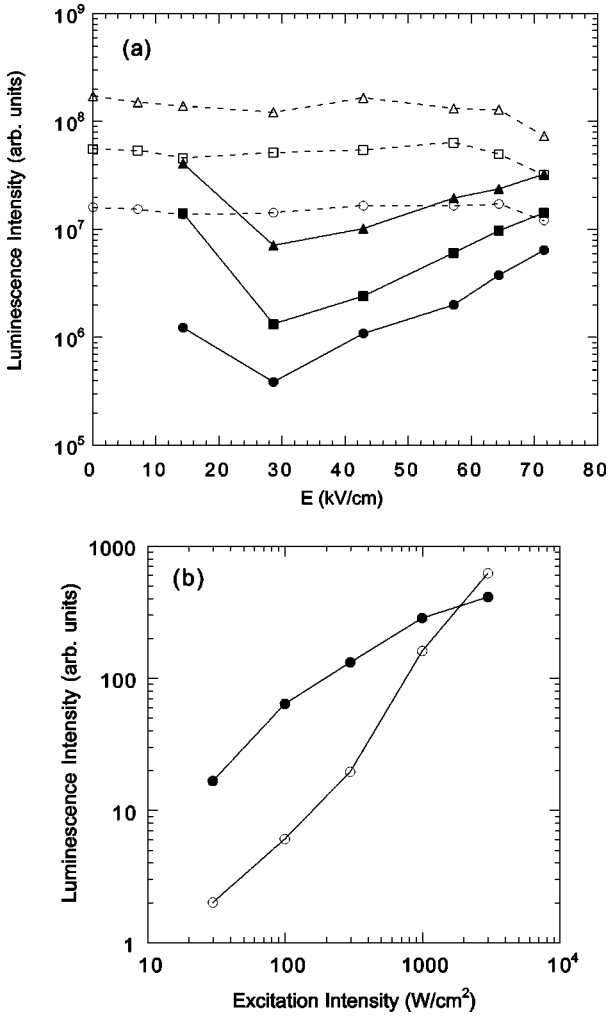

FIG. 4. (a) Total integrated intensity of the two luminescence lines from the coupled quantum wells as a function of electric field, at $T=2$ K, for three laser powers, at excitation wavelength 620 nm. Dashed lines: indirect exciton luminescence; solid lines: direct exciton luminescence. Triangles: 300 W/cm^2; squares: 100 W/cm^2; circles: 30 W/cm^2. (b) Relative intensity of the two luminescence lines from the coupled quantum wells as a function of excitation intensity, for the same conditions as in (a), at an electric field of 58 kV/cm. As seen in this figure, the direct exciton line becomes brighter than the indirect exciton line at high density and high electric field.

teractions between the excitons at high density, but two observations argue against this. First, the direct excitons, which are also polarized by the electric field and therefore also have strongly repulsive interactions with each other and with the indirect excitons, do not shift upward in energy at all; at high density, the direct line actually shifts slightly to the red, presumably due to lattice heating which causes the band gap to decrease. Although the direct excitons are smaller and therefore their interactions should have shorter range, one would expect that if the densities are high enough to give a mean-field blueshift of the indirect excitons, the direct excitons should also show some shift. Second, the initial short lifetime of the direct excitons can be understood as an effect of screening. If the effective electric field felt by the direct excitons is lower at early times, their lifetimes will be shorter, since the long radiative lifetime of both the direct and indirect excitons is due to the spatial separation of the electron and hole brought about by the electric field.

The early-time behavior of the two lines seen in Fig. 2 can therefore be understood in the following way: the indirect excitons have a slow initial rise time at high density because their luminescence is shifted to higher energies, out of the spectral range of our measurement, and therefore they do not enter the spectral range of our measurement until late times, while the direct excitons plotted in Fig. 2(a) have a short initial lifetime due to the screening of the electric field, but eventually have a long radiative lifetime since both the direct and the indirect excitons have spatially separated electrons and holes.

It comes as a surprise, however, that the upper, direct exciton luminescence has such a long overall lifetime at late times, since they can presumably couple down to the lower, indirect exciton state. Their population is clearly not in thermal equilibrium with the lower, indirect exciton level at high applied field, since the energy separation of the levels is several hundred times k_BT. The fact that the upper line has a lifetime comparable to that of the lower line at late times implies that the rate for converting from direct into indirect excitons is very slow at high electric field.

Figure 4(a) shows the relative intensity of the two lines as a function of applied field for three different laser powers. At zero electric field, the upper line can not be distinguished from the lower line. As the field is increased, the two lines

become distinguishable, and the intensity of the upper exciton line falls dramatically, as expected for populations of the excitons in thermal equilibrium.[31] As the applied field continues to increase, however, the upper luminescence line becomes brighter, until it actually overwhelms the light emission from the lower line. This effect has been observed before[32] and has been explained in terms of the symmetries of the states—at low electric field, the upper line corresponds to a forbidden symmetric-antisymmetric transition, which becomes more allowed as the electric field increases. As shown in Fig. 4(b), the intensity of the upper line increases superlinearly with laser intensity, while the lower line increases sublinearly. This can be understood in terms of the decrease of the direct exciton lifetime at high density, as follows. Since the laser photons create free carriers with high energy (but not high enough to cross over the pure AlAs barriers) both the direct and indirect exciton states are initially populated. At high electric field and high carrier density, the rate of conversion of the direct excitons to indirect excitons is slow compared to their rate of radiative decay, so that recombination into photons becomes the dominant decay mechanism for the direct excitons. At early times, this recombination rate occurs more quickly when the electric field is screened out, as discussed above, causing relatively more direct excitons to convert into photons instead of indirect excitons. Since the screening depends strongly on the carrier density, the intensity of the direct exciton luminescence increases superlinearly with laser power, at the expense of the indirect exciton population.

As seen in Fig. 3(a), the indirect exciton line has significant homogeneous broadening at early times at high carrier density; the direct exciton line has essentially the same broadening at the same times. At late times and at low temperatures, several peaks approximately 3–5 meV apart appear in the indirect exciton luminescence, which have been seen before (e.g., Refs. 33, 34) in high-quality quantum well structures and attributed variously to monolayer plateaus and excitons bound to impurities. At late times and at low temperature and low excitation density, the indirect luminescence decreases to a full width at half maximum of about 1 meV. In other words, although monolayer islands may exist in these samples, which give energy variations of around 3 meV for our well width of 60 Å,[33] they do not prevent the excitons from flowing to the lowest monolayer plateaus (the regions at which the quantum wells are widest) at late times. We take the measured width of 1 meV as the measure of inhomogeneous broadening due to alloy disorder or residual stresses in the sample. We found that if the back surface of the substrate is polished after the quantum wells have been grown, this inhomogeneous broadening increases dramatically, up to 10 meV, presumably due to residual stresses introduced in the polishing process. At best we could reduce this to around 5 meV after etching and annealing. Since, as discussed in the next section, we need a polished substrate for our experiment, this led us to start with a substrate polished on both sides before the quantum wells were deposited. The quantum wells grown by molecular beam epitaxy on the substrates polished on both sides also had inhomogeneous broadening of approximately 1 meV, as measured by the late-time photoluminescence linewidth.

The interaction of the free carriers, direct excitons and indirect excitons seen here leads to a highly nonlinear system in which both the wavelength and the intensity of the photons impinging on the sample strongly affects the spectral width and position of the absorption and emission lines. We can imagine numerous possibilities for utilizing these effects for nonlinear optics. Our interest at present, however, is in the behavior of the indirect excitons at low temperature in quasiequilibrium. The above effects imply that if the screening at high density cannot be eliminated, we must either use low laser power or observe the luminescence at least 50 ns after the laser pulse in order to see nearly equilibrium exciton levels.

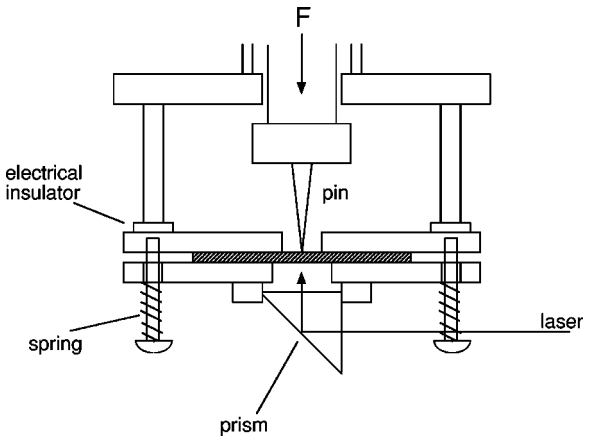

FIG. 5. Experimental geometry for applying inhomogeneous strain and electric field to the samples. The pin is pressed against the sample with approximately 5 lb of force.

III. THE HARMONIC POTENTIAL TRAP

As mentioned above, previous experiments[16] have succeeded in creating a harmonic potential for excitons in bulk semiconductors via applied inhomogeneous stress. Creating a harmonic potential for excitons in GaAs quantum wells is nontrivial, however. Since GaAs has a large hydrostatic deformation potential, any stress geometry which leads to a significant hydrostatic compression will cause a large shift of the excitons to *higher* energy. In the case of a purely uniaxial stress, it is well known[35] that the exciton energy shifts upward with increasing stress.

Figure 5 shows the experimental geometry which allows us to create a harmonic-potential minimum for the indirect excitons. The quantum well sample is clamped between two metal plates, each with a small hole, and a pin is pressed against the GaAs substrate, which has been polished on both surfaces prior to the MBE fabrication. The pin creates a shear strain maximum in the quantum wells, as well as a slight hydrostatic expansion, each of which leads to an energy minimum for the excitons via the Pikus–Bir deformation Hamiltonian[36] for GaAs,

$$H_{\mathrm{PB}} = a(\epsilon_{xx}+\epsilon_{yy}+\epsilon_{zz}) + 3b[(J_x^2 - J^2/3)\epsilon_{xx} + \mathrm{c.p.}] + \frac{6d}{\sqrt{3}}\left[\frac{1}{2}(J_xJ_y + J_yJ_x)\epsilon_{xy} + \mathrm{c.p.}\right], \quad (1)$$

where a is the hydrostatic deformation potential and b and d are the shear deformation potentials for GaAs,[37] and the J's

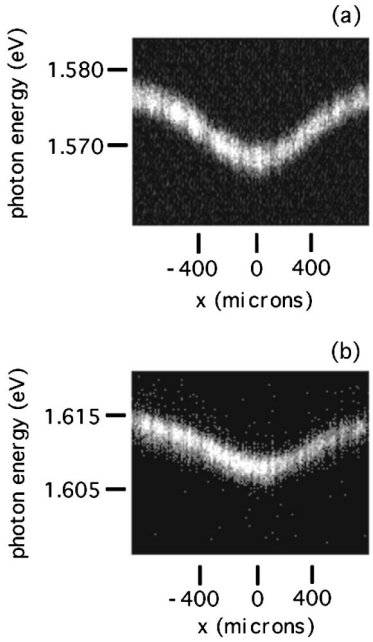

FIG. 6. (a) Time-integrated image through an imaging spectrometer of the indirect exciton luminescence as the laser spot is scanned across the surface of the quantum well sample with 43 kV/cm applied field. The point of lowest energy corresponds to the point directly below the tip of the pin shown in Fig. 5. (b) Time-integrated image for the same conditions but zero applied field. As seen in this comparison, the inhomogeneous electric field gives a contribution to the trap as large as that of the applied shear stress.

refer to the spin states of the valence band, $m=3/2$, $1/2$, $-1/2$, and $-3/2$. For a uniaxial strain along the z direction, this Hamiltonian corresponds to $E_{\rm PB}=3a\epsilon_{\rm hydro}\pm 3b\epsilon_{\rm shear}$, where $\epsilon_{\rm hydro}=\frac{1}{3}(\epsilon_{xx}+\epsilon_{yy}+\epsilon_{zz})$ and $\epsilon_{\rm shear}=(\epsilon_{zz}-\frac{1}{2}\epsilon_{xx}-\frac{1}{2}\epsilon_{yy})$. The use of a shear stress maximum to produce a potential energy minimum has been used for carriers in bulk semiconductors,[16,38,39] but in the present case, the *hydrostatic* term also makes a significant contribution to the exciton energy, as discussed below. Too much stress from the pin will cleave the sample, of course, but springs on the back of the sample help to prevent this, allowing a reproducible, controllable stress.

In addition, the pin is held at a fixed, negative voltage while the clamping plates are connected to ground. This causes a current to flow through the heavily doped substrate, so that the voltage across the quantum wells drops to zero far away from the pin. As seen in Fig. 1, higher electric field corresponds to lower energy for the indirect excitons, so that this effect also contributes to a potential energy minimum for the excitons below the pin.

The entire assembly is placed in liquid or gaseous helium, and the quantum wells are excited by a laser through the window of an optical cryostat by means of a prism attached to the lower metal plate. The force on the pin is controlled by a micrometer at the top of the cryostat, as in Ref. 39. Figure 6 shows time-integrated luminescence from a coupled quantum well sample taken with a CCD camera on the back of an imaging spectrometer as the laser spot is scanned across the surface of the sample. As seen in Fig. 6(a), a well depth of more than 10 meV can be created, compared to the inhomogeneous broadening in these samples of around 1 meV.

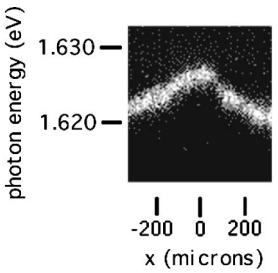

FIG. 7. Time-integrated image through an imaging spectrometer of the exciton luminescence as the laser spot is scanned across the surface of the quantum well sample with zero applied field, when the sample is pressed with a pin as in Fig. 5, but the bottom surface is placed flat on a glass slide.

When the voltage applied to the pin is set to zero, the same time-integrated scan gives Fig. 6(b), which shows that the effect of the variation in voltage is about the same as the effect of the applied stress.

The fact that a potential minimum occurs is strongly connected to the geometry which leaves the lower surface of the sample unconstrained. This leads to a local hydrostatic *expansion* of the sample, which lowers the energy of the excitons via the first term of Eq. (1). When the sample is placed on a glass slide, a local hydrostatic *compression* occurs. In this case, the positive shift in energy due to the hydrostatic deformation potential (which is approximately five times larger than the shear deformation potential[37]) cancels the negative shift due to the shear strain, leading to nearly no net shift and an energy *maximum* for the excitons below the pin, as seen in Fig. 7. Figure 8 shows numerical solutions of the static stress field equations for these two experimental geometries (the details of these calculations will be presented elsewhere[40]). In Fig. 8(a), the boundary conditions are the same as the experimental geometry of Fig. 6, in which the bottom surface is suspended freely over a small hole in the bottom plate, while Fig. 8(b) shows the solution of the same equations for the boundary conditions of Fig. 6, in which the bottom surface is held fixed. As seen in these plots, the sign of the hydrostatic strain changes sign from compression to expansion depending on the boundary conditions. The fact that the bottom surface is left suspended freely is therefore essential for the production of a harmonic potential trap for the excitons. We note that the horizontal, spatial scale of the image in Fig. 7 is much smaller than that of Fig. 6. This is because of the particular details of the way in which the deformation potential terms cancel, which will be discussed elsewhere.[40] The shift of exciton line depends sensitively on the deformation potentials, and therefore these experiments also allow us to measure ratios of the hydrostatic and shear deformation potentials in GaAs.[40]

In a harmonic potential minimum in two dimensions, the critical number for Bose condensation is given by

$$N_c=\sum_n n\frac{1}{e^{n\hbar\omega/k_BT}-1}$$

$$=\frac{(k_BT)^2}{(\hbar\omega_0)^2}\int \epsilon\, d\epsilon\frac{1}{e^{\epsilon}-1}=1.8\frac{(k_BT)^2}{(\hbar\omega_0)^2}, \qquad (2)$$

where $\omega_0=(\alpha/m)^{1/2}$. The shape of the well shown in Fig. 6(a) corresponds to a force constant of $\alpha=65\ \mathrm{meV/mm^2}$,

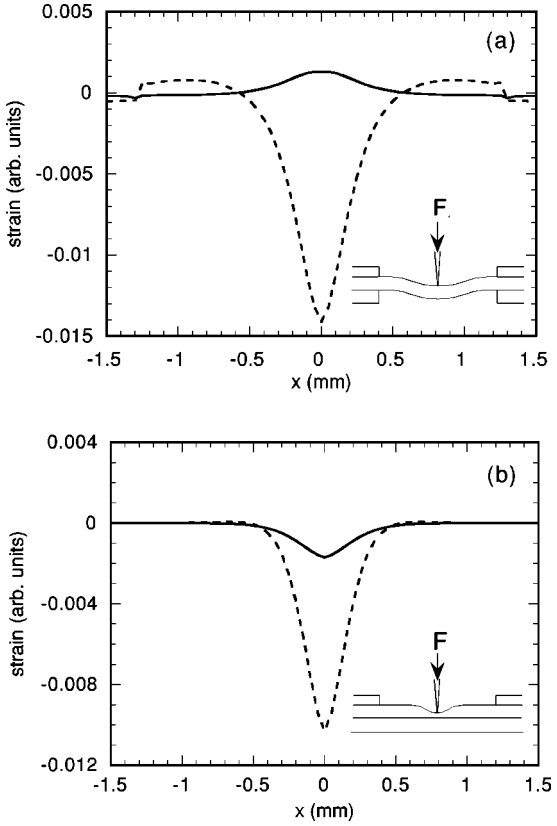

FIG. 8. (a) Numerical solution of the static field equations for the elastic constants of GaAs and the experimental geometry of Fig. 5 for a 500 μm thick substrate, when the bottom surface is suspended freely over a 2.5 mm hole, as illustrated in the inset (the boundary conditions of the data in Fig. 6). Solid lines: the hydrostatic strain $(\epsilon_{xx}+\epsilon_{yy}+\epsilon_{zz})$ on the bottom surface of the sample. Dashed lines: the shear strain $3(\epsilon_{zz}-\epsilon_{xx}/2-\epsilon_{yy}/2)$. (b) Solution for the same geometry and the same applied force, but the bottom surface constrained to zero displacement, as illustrated in the inset (the boundary conditions of the data in Fig. 7).

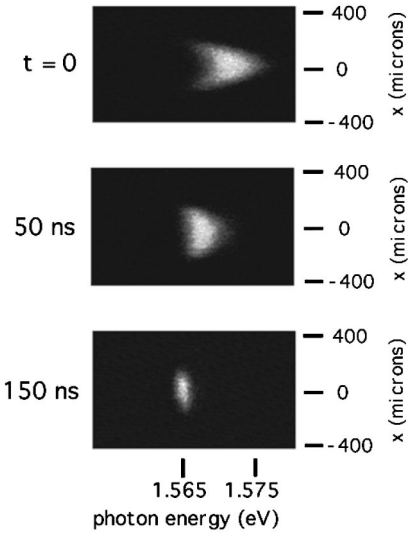

FIG. 9. Time-gated images of the indirect exciton luminescence for various delays following a short laser pulse in the center of the well shown in Fig. 6(a), using a time-gated Princeton CCD camera on the back of an imaging spectrometer. The time gate width for these images was 50 ns, although time resolution as low as 5 ns is possible with this system.

approximating $U=\alpha x^2/2$ in the center of the trap. For a temperature of 2 K and exciton mass on the order of the electron mass, this critical number is approximately 10^7. For comparison, a single laser pulse from our dye laser contains more than 10^{11} photons. By contrast, a three-dimensional well with the same force constant would require a critical number at the same temperature of $1.2[(k_BT)^3/(\hbar\omega_0)^3]=3\times10^{10}$, which leaves little room for loss processes or inefficient photon absorption.

One can also estimate whether the indirect excitons will remain *weakly interacting* at critical density in this well. The effective area of the equilibrium gas in this well at $T=2$ K is found approximately by equating the thermal energy with the potential energy, i.e., $k_BT=\frac{1}{2}\alpha x^2$, which implies $x=\sqrt{2k_BT/\alpha}\simeq80\ \mu$m. For 10^7 excitons this implies an interparticle spacing of $\sqrt{\pi(80\ \mu\text{m})^2/10^7}=44$ nm. By comparison, the effective hardcore size of the indirect excitons is of the order of the total width of the coupled quantum wells, which in this case is 16 nm. Since this is well below the interparticle spacing, the indirect excitons should be adequately described by the theory of the weakly interacting Bose gas.

Despite the promise of the above estimates, we have not yet seen evidence for Bose effects in this well. As discussed in Sec. II, the screening at high carrier density leads to several undesirable effects. First, it causes shorter exciton lifetime, which reduces the total density. Second, the blueshift of the indirect exciton line is spatially inhomogeneous, leading to an energy *maximum* in the center of the laser pulse where the carrier density is the highest. Figure 9 shows three time-gated images of the indirect exciton luminescence following a short laser pulse in the center of the well shown in Fig. 6(a). As seen in this figure, at early time the excitons in the center of the laser spot have higher blueshift due to the higher carrier density. Only at late times, after the exciton density has fallen significantly, does this maximum disappear.

It is not clear from these experiments whether the screening is mostly due to free carriers or the excitons themselves. If it is mostly free carriers in the quantum wells due to the large excess energy (300 meV) of the laser photons at 660 nm, then this can be eliminated by near-resonant excitation. We expect that the contribution to screening by the excitons should be minimal at densities at or below the density calculated above for a weakly interacting gas. If the screening we observe is due primarily to excitons and not due to free carriers, then this indicates that we have achieved very high densities in these quantum wells, well above what is necessary for Bose condensation, albeit at a high effective temperature.

While we cannot directly measure the exciton temperature, we can estimate the exciton temperature from the spectrum of the band-edge luminescence from the GaAs substrate for the first few nanoseconds after the laser pulse. Straight-line fits to the logarithm of the high-energy luminescence of the free carriers in the substrate give temperatures of greater than 150 K for times up to 6 ns after an intense laser pulse, with a cooling rate of about 20 K/ns, when the sample is immersed in liquid helium. This makes it likely that the ex-

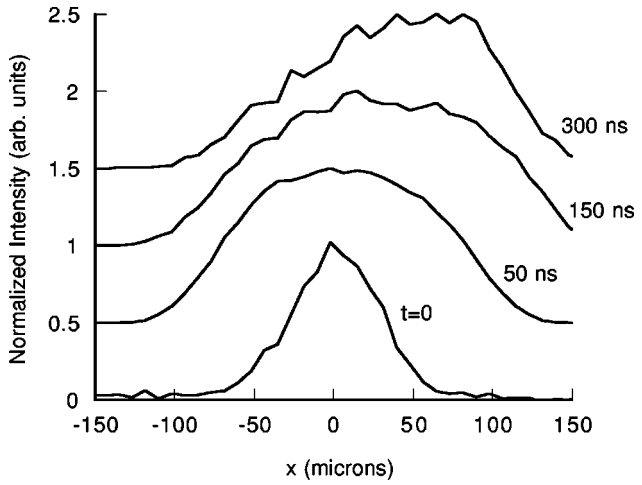

FIG. 10. Spatial profiles of the luminescence from the coupled quantum well structure at various times after a short (5 ps) laser pulse. The laser is focused about 400 μm from the center of the trap shown in Fig. 6. As seen in this figure, the indirect excitons drift toward the center of the well due to the gradient in potential energy. The $t=0$ profile, which mirrors the laser focus, is obtained from the profile of the hot free-carrier luminescence from the substrate.

citon gas does not cool to the lattice temperature until well after 50 ns, since the cooling rate slows at late times. Changing to longer-wavelength, near-resonant excitation may significantly reduce this effective temperature.

IV. DIFFUSION OF INDIRECT EXCITONS

Another important issue in attempting to see Bose effects in these traps is whether the excitons can diffuse far enough to equilibrate in the trap within their lifetime. We can measure the diffusion constant of the excitons via time-resolved spatial imaging of the luminescence as in Fig. 9.

Figure 10 shows the spatial profile of the indirect exciton luminescence at various times after a laser pulse has created them about 400 μm from the center of the well. Each of these profiles has been obtained by integrating over the total spectrum (the x axis) of a time-gated image similar to one of those shown in Fig. 9. The $t=0$ profile, however, corresponds to the luminescence profile of the hot carrier luminescence of the substrate, since this gives an accurate measure of the laser spot size. The earliest recorded indirect exciton luminescence is always much broader than this at high laser power, indicating an explosive expansion within just a few nanoseconds.

Care must be taken to deduce a correct diffusion constant from these data. Although the expansion from $t=0$ to 50 ns seen in Fig. 10 indicates a diffusion constant of 1000 cm^2/s, there exists an effect which could give a false indication of fast expansion. At high carrier density, the screening significantly alters the exciton level, leading to a shorter lifetime for the direct excitons and presumably also for the indirect excitons. If the lifetime is shorter in regions of high exciton density near the center of the spot, deducing the diffusion constant from the spatial profile of the exciton luminescence will give a false measurement, since the full width at half maximum would increase in this case even if the excitons did not diffuse at all. At times greater than 50 ns after the laser pulse, however, we can be certain that the exciton all have a single lifetime, since as seen in Figs. 2 and 3, the effect of screening ceases by then. We find that the diffusion constant 50 ns after an intense laser pulse is 400 cm^2/s, falling to around 1 cm^2/s at late times. The diffusivity of the excitons is strongly dependent on the exciton density, as also seen in Ref. 22, presumably due to localization of the excitons at low densities.

The fast expansion seen in Fig. 10 at early time is also seen when there is no trap for the excitons, i.e., with zero applied stress and a homogeneous electric field. As one can see in Fig. 10, however, the potential energy gradient in the trap also leads to a drift of the excitons. From this we can calculate an effective mobility for the excitons. To do this we first estimate an effective ''charge'' for the excitons, by noting that a voltage of 3 V applied to the surface of the sample leads to a Stark shift of the indirect excitons of about 60 meV for our sample geometry. The excitons therefore respond to a voltage as if they had a charge of $0.02e$. The measured diffusion constant of the excitons of 400 cm^2/s at a temperature of about 120 K therefore implies an effective mobility for the excitons of 800 $\mathrm{cm}^2/\mathrm{V\,s}$. This number obviously depends on the sample geometry since the effective ''charge'' of the indirect excitons depends on the barrier thicknesses, which control the electric field felt by the excitons in the quantum wells; for thinner barriers this number will be higher.

Overall, the maximum expansion of the excitons is around 100 μm. Although this is greater than the equilibrium spatial width of the exciton gas at 2 K calculated above, this expansion only occurs at high carrier density, which in these experiments also implies temperatures of around 100 K, as mentioned above. This also indicates the importance of reducing the effective temperature of the excitons by using near-resonant excitation.

V. CONCLUSIONS

These experiments open up a new path for experiments on excitons in two dimensions with a controlled volume. The depth of the harmonic potential which we create can be controlled during the experiment via the applied voltage and stress.

At this point, there is little apparent difficulty in achieving the densities needed for Bose condensation of excitons in these wells. The remaining problems are first, getting the temperature of the excitons low enough to condense (but not too low, or else the excitons will most likely become localized), and second, operating in a regime where screening is not important. We have seen that the effect of screening on the exciton states is extremely important in these experiments. We have not determined whether this screening is mostly due to free carriers or the excitons themselves; eliminating the free-carrier population by using laser excitation near the exciton resonance will help to determine this, in addition to allowing lower exciton temperatures.

In addition to changing to near-resonant excitation, we can also pursue Bose condensation of excitons in this geometry by adding a strong magnetic field, which will reduce the spin degeneracy of the excitons, forcing higher numbers of particles into fewer states, and also creating a more strongly

repulsive interaction between the excitons. Several authors[41–43] have argued that magnetic field will enhance Bose effects of excitons; experimentally, Ref. 9 reported a sharp increase of diffusivity of indirect excitons above a critical threshold of magnetic field.

The slow conversion of direct excitons to indirect excitons at high applied field may also present a barrier to Bose condensation, since at high density and high voltage, a large fraction of the excited carriers appear to remain in the direct exciton state, which has short lifetime. The process of conversion of direct to indirect excitons, in particular its dependence on voltage, is not well understood, and further work to determine this mechanism is important.

Finally, we note that the method we have used here to trap the excitons may have other applications. Since excitons are charge neutral, they do not respond to electric field, and it is therefore difficult to control their motion. We have shown that the motion of excitons in heterostructures can be controlled over distances up to 100 μm via inhomogeneous electric field. Variation of the voltage across the quantum wells can be accomplished by depositing resistive patterns on the surface via photolithography. Small ''wires'' for excitons can therefore be created which carry excitons from place to place in response to electric fields, with effective mobilities on the order of 1000 $cm^2/V\,s$ at 100 K.

We also note that the method of producing a harmonic potential using inhomogeneous strain can also be applied to other, nonexcitonic systems such as the two-dimensional electron gas (2DEG). Although the shear strain term in the Pikus-Bir Hamiltonian only applies to the valence states, the hydrostatic deformation term is believed to arise mostly from the conduction band.[44] Therefore the hydrostatic expansion which occurs in our stress geometry will lead to an energy minimum for free conduction electrons in GaAs. This allows an extra ''gate,'' independent of voltage, which can be used to produce a spatially localized 2DEG in a well-defined harmonic potential.

ACKNOWLEDGMENTS

This work has been supported by the National Science Foundation under Grant No. DMR-97-22239. One of the authors (D.S.) thanks the Research Corporation for financial support. We thank I. Hancu for early contributions to these experiments, and S. D. Baranovskii, M. Cardona, L. M. Smith, V. B. Timofeev, and V. I. Yudson for helpful conversations.

*Electronic address: snoke@vms.cis.pitt.edu

[1] V. B. Timofeev, V. D. Kulakovskii, and I. V. Kukushkin, Physica B&C **117/118**, 327 (1983).
[2] N. Peyghambarian, L. L. Chase, and A. Mysyrowicz, Phys. Rev. B **27**, 2325 (1983).
[3] D. W. Snoke, J. P. Wolfe, and A. Mysyrowicz, Phys. Rev. B **41**, 11 171 (1990).
[4] D. W. Snoke, Jia-Ling Lin, and J. P. Wolfe, Phys. Rev. B **43**, 1226 (1991).
[5] J. L. Lin and J. P. Wolfe, Phys. Rev. Lett. **71**, 1223 (1993).
[6] M. Hasuo, N. Nagasawa, T. Itoh, and A. Mysyrowicz, Phys. Rev. Lett. **70**, 1303 (1993).
[7] T. Fukuzawa *et al.*, Phys. Rev. Lett. **64**, 3066 (1990).
[8] L. V. Butov, A. Zrenner, G. Abstreiter, G. Böhm, and G. Weimann, Phys. Rev. Lett. **73**, 304 (1994).
[9] L. V. Butov, A. Zrenner, M. Hagn, G. Abstreiter, G. Böhm, and G. Weimann, Surf. Sci. **361/362**, 243 (1996).
[10] E. Fortin, S. Fafard, and A. Mysyrowicz, Phys. Rev. Lett. **70**, 3951 (1993).
[11] T. Goto, M. Y. Shen, S. Koyama, and T. Yokouchi, Phys. Rev. B **55**, 7609 (1997).
[12] M. Y. Shen, T. Yokouchi, S. Koyama, and T. Goto, Phys. Rev. B **56**, 13 066 (1997).
[13] J. C. Kim and J. P. Wolfe, Phys. Rev. B **57**, 9861 (1998).
[14] M. H. Anderson, J. R. Ensher, M. R. Matthews, C. E. Weiman, and E. A. Cornell, Science **269**, 198 (1995).
[15] K. B. Davis, M. O. Mewes, M. R. Andrews, N. J. Van Druten, D. S. Durfee, D. M. Kurn, and W. Ketterle, Phys. Rev. Lett. **75**, 3969 (1995).
[16] D. P. Trauernicht, J. P. Wolfe, and A. Mysyrowicz, Phys. Rev. B **34**, 2561 (1986).
[17] See, e.g., K. Huang, in *Bose-Einstein Condensation*, edited by A. Griffin, D. W. Snoke, and S. Stringari (Cambridge University Press, Cambridge, 1995).
[18] J. Fernández-Rossier, C. Tejedor, and R. Merlin, Solid State Commun. **108**, 473 (1998).
[19] P. Nozierés, in *Bose-Einstein Condensation* (Ref. 17).
[20] X. J. Zhu, P. B. Littlewood, and T. M. Rice, Phys. Rev. Lett. **74**, 1633 (1995).
[21] J. A. Kash, M. Zachau, E. E. Mendez, J. M. Hong, and T. Fukuzawa, Phys. Rev. Lett. **66**, 2247 (1991).
[22] G. D. Gilliland, D. J. Wolford, G. A. Northrop, M. S. Petrovic, T. F. Kuech, and J. A. Bradley, J. Vac. Sci. Technol. B **10**, 1959 (1992).
[23] S. A. Moskalenko, Fiz. Tverd. Tela (Leningrad) **4**, 276 (1962) [Sov. Phys. Solid State **4**, 199 (1962)]; V. A. Gergel, R. F. Kazarinov, and R. A. Suris, Zh. Eksp. Teor. Fiz. **53**, 544 (1967) [Sov. Phys. JETP **26**, 354 (1968)]; **54**, 298 (1968) [**27**, 159 (1968)]; L. V. Keldysh, in *Problems of Theoretical Physics* (Nauka, Moscow, 1972), pp. 433–444; E. Hanamura and H. Haug, Solid State Commun. **15**, 1567 (1974).
[24] S. G. Tikhodeev, Phys. Rev. Lett. **78**, 3225 (1997); G. A. Kopelevich, S. G. Tikhodeev, and N. A. Gippius, Zh. Éksp. Teor. Fiz. **109**, 2189 (1996) [JETP **82**, 1180 (1996)].
[25] Th. Östreich, T. Portengen, and L. J. Sham, Solid State Commun. **100**, 325 (1996).
[26] B. Laikhtman, Europhys. Lett. **43**, 53 (1998).
[27] V. Negoita, D. W. Snoke, and K. Eberl, in *Proceedings of the 24th International Conference on Physics and Semiconductors*, Jerusalem (World Scientific, Singapore, 1998).
[28] S. R. Andrews, C. M. Murray, R. A. Davies, and T. M. Kerr, Phys. Rev. B **37**, 8198 (1988).
[29] A. M. Fox, D. A. B. Miller, G. Livescu, J. E. Cunningham, and W. Y. Jan, Phys. Rev. B **44**, 6231 (1991).
[30] Y. Kato, Y. Takahashi, S. Fukatsu, Y. Shiraki, and R. Ito, J. Appl. Phys. **75**, 7476 (1994).
[31] M. R. Reshotko, L. D. Shvartsman, and J. E. Golub, Phys. Rev. B **50**, 4692 (1994).
[32] Y. J. Chen, E. S. Koteles, B. S. Elman, and C. A. Armiento, Phys. Rev. B **36**, 4562 (1987).
[33] L. Schrottke, H. T. Grahn, and K. Fujiwara, Phys. Rev. B **56**, 13 321 (1997).

[34] L. Schrottke, J. Ringling, H. T. Grahn, and K. Fujiwara, in *Proceedings of the 24th International Conference on Physics and Semiconductors* (Ref. 27).
[35] F. H. Pollak and M. Cardona, Phys. Rev. **172**, 816 (1968).
[36] See, e.g., P. Y. Yu and M. Cardona, *Fundamentals of Semiconductors* (Springer, Berlin, 1996), p. 119.
[37] *Landolt-Börnstein Numerical Data and Function Relationships in Science and Technology*, edited by O. Madelung and M. Schulz (Springer, Berlin, 1987), Vol. III.22a.
[38] R. S. Markiewicz, J. P. Wolfe, and C. D. Jeffries, Phys. Rev. B **15**, 1988 (1977).
[39] P. L. Gourley and J. P. Wolfe, Phys. Rev. B **24**, 5970 (1981).
[40] V. Negoita, D. W. Snoke, and K. Eberl (unpublished).
[41] A. V. Korolev and M. A. Liberman, Solid State Commun. **98**, 49 (1996); Phys. Rev. Lett. **72**, 270 (1994).
[42] D. Paquet *et al.*, Phys. Rev. B **32**, 5208 (1985).
[43] I. V. Lerner and Yu. E. Lozovik, Zh. Eksp. Teor. Fiz. **80**, 1488 (1981) [Sov. Phys. JETP **53**, 763 (1981)].
[44] E.g., M. Cardona and N. E. Christensen, J. Vac. Sci. Technol. B **6**, 1285 (1988).